Research article

Nicholas V. Proscia, Harishankar Jayakumar, Xiaochen Ge, Gabriel Lopez-Morales, Zav Shotan, Weidong Zhou, Carlos A. Meriles* and Vinod M. Menon*

Microcavity-coupled emitters in hexagonal boron nitride

https://doi.org/10.1515/nanoph-2020-0187
Received March 11, 2020; accepted April 21, 2020

Abstract: Integration of quantum emitters in photonic structures is an important step in the broader quest to generate and manipulate on-demand single photons via compact solid-state devices. Unfortunately, implementations relying on material platforms that also serve as the emitter host often suffer from a tradeoff between the desired emitter properties and the photonic system practicality and performance. Here, we demonstrate "pick and place" integration of a Si_3N_4 microdisk optical resonator with a bright emitter host in the form of ~20-nm-thick hexagonal boron nitride (hBN). The film folds around the microdisk maximizing contact to ultimately form a hybrid hBN/Si_3N_4 structure. The local strain that develops in the hBN film at the resonator circumference deterministically activates a low density of defect emitters within the whispering gallery mode volume of the microdisk. These conditions allow us to demonstrate cavity-mediated outcoupling of emission from defect states in hBN through the microdisk cavity modes. Our results pave the route toward the development of chip-scale quantum photonic circuits with independent emitter/resonator optimization for active and passive functionalities.

Keywords: 2D materials; color center; hexagonal boron nitride; microcavities; quantum emission; strain.

1 Introduction

Cavity-coupled solid-state quantum emitters serve as a test bed for numerous cavity quantum electrodynamics (CQED) experiments [1–4], and are primarily utilized as a source of non-classical light [5, 6], and for photonic quantum information processing [7] and communication [8]. Recent practical demonstrations have exploited a variety of solid-state quantum emitter systems including quantum dots [9], single molecules [10], atomically thin transition metal dichalcogenides (TMDs) [11–15], and point defects in wide bandgap materials such as diamond [16–18] and silicon carbide [19]. While differing applications impose specific requirements, bright coherent sources operating at room temperature and tunable over a broad spectral range are invariably desirable. Recently, point defects in hexagonal boron nitride (hBN) have emerged as a versatile source of quantum light with unique capabilities for integration in scalable nanophotonic structures operating under ambient conditions [20]. Emitters in monolayer and multilayer hBN have been shown to emit photons at very high rates in the visible wavelength range [21, 22], featuring narrow-linewidth zero-phonon lines (ZPLs) [23] and large Debye-Waller factors [20]. Current research efforts are focused on determining the defect composition [24], tunability [25, 26], deterministic creation [27] and emitter activation [28], and integration with photonic structures [29, 30]. In particular, coupling to silicon photonic structures and chip-scale photonic cavities, crucial for high-fidelity photon manipulation and routing, remains an outstanding challenge.

One possible approach to cavity-coupled SPEs in hBN is via fabrication of photonic cavity structures from a bulk crystal. This technique has been successfully implemented

*Corresponding authors: Carlos A. Meriles and Vinod M. Menon, Department of Physics, CUNY-City College of New York, New York, NY, 10031, USA; and Department of Physics, CUNY-Graduate Center, New York, NY, 10016, USA, E-mail: cmeriles@ccny.cuny.edu (Carlos A. Meriles); vmenon@ccny.cuny.edu (Vinod M. Menon)
Nicholas V. Proscia and Gabriel Lopez-Morales: Department of Physics, CUNY-City College of New York, New York, NY, 10031, USA; Department of Physics, CUNY-Graduate Center, New York, NY, 10016, USA, E-mail: nproscia1@ccny.cuny.edu (N.V. Proscia), glopezmorales@gradcenter.cuny.edu (G. Lopez-Morales). https://orcid.org/0000-0003-4307-7537 (N.V. Proscia)
Harishankar Jayakumar and Zav Shotan: Department of Physics, CUNY-City College of New York, New York, NY, 10031, USA, E-mail: hjayakumar@ccny.cuny.edu (H. Jayakumar), zav.shotan@gmail.com (Z. Shotan)
Xiaochen Ge and Weidong Zhou: Department of Electrical Engineering, University of Texas at Arlington, Arlington, TX, 76019, USA, E-mail: gexcster@gmail.com (X. Ge), wzhou@uta.edu (W. Zhou)

Open Access. © 2020 Nicholas V. Proscia et al., published by De Gruyter. This work is licensed under the Creative Commons Attribution 4.0 Public License.

with epitaxial quantum dots [1, 2], and with color centers in diamond [4, 16] and silicon carbide [19]. Recently, Kim et al. [31] extended this strategy to hBN reporting the fabrication of a photonic crystal cavity from a bulk hBN substrate. The two-dimensional (2D) nature of this van der Waals material, however, makes it compatible with 'pick-and-place' techniques designed to bring a thin, emitter-hosting layer in close contact with the target photonic structure. The advantage in this 'hybrid' approach is that the emitter properties (e. g., brightness, spin and/or optical lifetimes) and the photonic system performance (e. g., photon losses/quality factors) can be optimized independently. Further, the ability to choose the substrate material from a broader set circumvents complications arising from systems that cannot be produced in wafer size, are hard to process, or require fabrication steps affecting the emitter performance. These properties were recently exploited to demonstrate coupling between hBN emitters and a plasmonic resonator [30, 32].

Here, we "pick and place" the hBN film on a silicon nitride (Si_3N_4) microdisk optical cavity. The hBN film wraps around the microdisk and the undercut to reproduce the local topography. Carrier capture via strain-induced potentials selectively turns the intrinsic hBN point defects at the resonator perimeter into bright emitters without the need for ion implantation or high-temperature annealing. This 'defect activation' mechanism [28, 33] seamlessly produces emitters within the evanescent field of the microdisk cavity modes. Exploiting this configuration, we demonstrate coupling of the emitter ensemble to the whispering gallery modes (WGMs) of the microdisk cavity.

2 Materials and methods

2.1 Sample preparation

The microdisks were fabricated from a 112 nm Si_3N_4 layer on a silicon substrate. The stoichiometric silicon nitride film was deposited on the silicon substrate by low pressure chemical vapor deposition (LPCVD). The microdisk structures were patterned on ZEP520A resist by electron beam lithography (EBL) and etched onto the Si_3N_4 layer by inductively coupled plasma reactive ion etching (ICP-RIE) using a gas combination of SF_6, CHF_3 and He. The silicon substrate was then undercut by another ICP-RIE process with SF6 to form the suspended Si_3N_4 microdisk structure. Finally, the remaining e-beam resist was removed by N-Methyl-2-pyrrolidone (NMP) followed by O_2 plasma ashing.

The hBN used in this study was a 20-nm-thick film grown on copper via chemical vapor deposition obtained from Graphene Supermarket. The transfer protocol was a standard wet transfer process described in detail in Ref. [29]. The resulting hBN flake covered an area of 25 mm^2. The hBN-microcavity samples studied in this report did not undergo any high temperature annealing.

2.2 Optical characterization

Optical characterization of the sample was accomplished via a custom-built confocal microscope in the collinear excitation collection geometry. A dual scanning system was employed to both galvo-scan the collection spot and excitation beam across the sample and raster-scan the sample via a piezo stage across a fixed laser excitation and collection path. An infinity-corrected 0.83 numerical aperture (NA) Olympus objective and a 100X, 0.75 NA Zeiss objective was used to collect the micro-PL. The excitation source was a 500 fs pulsed fiber laser with a repetition rate of 80 MHz operating at 510 nm (Toptica FemtoFiber pro TVIS); the focused spot size had a diameter of ~1 μm. A 532 nm angle-tuned laserline filter (Thorlabs FL532-10) was used to remove unwanted spectral modes of the laser. Angle-tuned (edged from ~540 to ~640 nm) shortpass and longpass filters (Semrock TSP01 & Semrock TLP01, respectively) were used to cut off the reflected laser excitation as well as selectively isolate the MD cavity modes for further analysis. Lifetime measurements were performed using an avalanche photo diode (APD) (Micro Photon Devices PDM series) with 50 ps jitter, and a Picoquant – Picoharp-300 time tagger. An 80–20 emission beam-splitter provided real-time spectral analysis with an iHR-320 Horiba spectrometer.

3 Results and discussion

3.1 Hybrid photonic microcavity

Figure 1 shows a ~20 nm-thick flake of hBN on an array of silicon nitride (Si_3N_4) pedestal microdisks supporting WGM resonances. These cavities are designed to sustain in-plane transverse electric (TE) WGMs in the visible wavelength range between 550 and 650 nm, roughly matched to the emission wavelength of the hBN emitters. All microdisks feature a tip on its periphery to out-couple the scattered resonator modes into a high NA confocal microscope objective (Supplementary Figure 1). The cavity mode Q-factors of the bare microdisks were ~1000 (~3500) for the 3 μm (4 μm) diameter resonators and found to decrease by about a factor of 4 once encapsulated with hBN. The cavity free spectral range (FSR) goes from ~20 to ~15 nm within the investigated spectral band. Further details on the microdisk fabrication and optical properties can be found in Supplementary Note 1.

Upon hBN transfer to the resonator array, the composite hBN/Si_3N_4 structures that emerge take different geometries, as illustrated in the scanning electron microscopy (SEM) images of Figure 1. For example, on occasions we find that the flake falls almost vertically at the microdisk perimeter to make contact with the undercut etch without noticeable damage ('tablecloth' geometry in Figure 1A), while at other times the film bridges the space between the microdisk and the surrounding resonator host crystal without undergoing

any visible distortion ('suspended' geometry in Figure 1B). Typically, the unsupported section of the film undergoes variable rupture at the resonator periphery (see, for example, Figure 1B and C), ultimately tearing apart completely to fold around the microdisk ('wrapped' geometry in Figure 1D). This type of hBN wrapping — seen in approximately one third of the microdisks — features a polygonal shape with 5 to 7 vertices, this number growing with the disk diameter (Figure 1E–G).

Of all configurations, here we focus on the latter, 'wrapped' microdisks where emitters tend to cluster near the disc periphery and thus lie proximal to the evanescent field of the WGM. This is shown in the scanning fluorescence image of Figure 2A, predominantly brighter in areas around the resonator circumference and outer contour of the undercut (see also accompanying SEM images in Figure 2B). Away from the out-coupling tip, the majority of the emission collected in the confocal scan is due to uncoupled hBN emission. Notice that the photon emission originates almost exclusively from hBN as the bare Si_3N_4 emission is over two orders of magnitude weaker. In particular, no photoluminescence (PL) is detected above the noise floor in sections where the hBN film is torn (Supplementary Figure S2, see also Figure 3B below).

We recently observed similar behavior in hBN films on arrays of SiO_2 micro-pillars — where bright defect emitters were selectively generated at the pillar sites — and showed that this response can be understood as a result of emitter activation driven by carrier capture in strain-induced potentials [28]. This same process is at work here with analogous folding-induced strain fields selectively activating the emission from defects near the resonator's periphery. This is particularly the case for the vertices of the polygonal folds where the hBN curvature and thus the accumulated strain is highest (see zoomed confocal image of Figure 2C and isometric SEM image in Figure 2D). We contrast this type of emitter engineering with that attained via hBN annealing at ~850 °C (Supplementary Figure 3), broadly used but largely non-deterministic in the resulting spatial distribution.

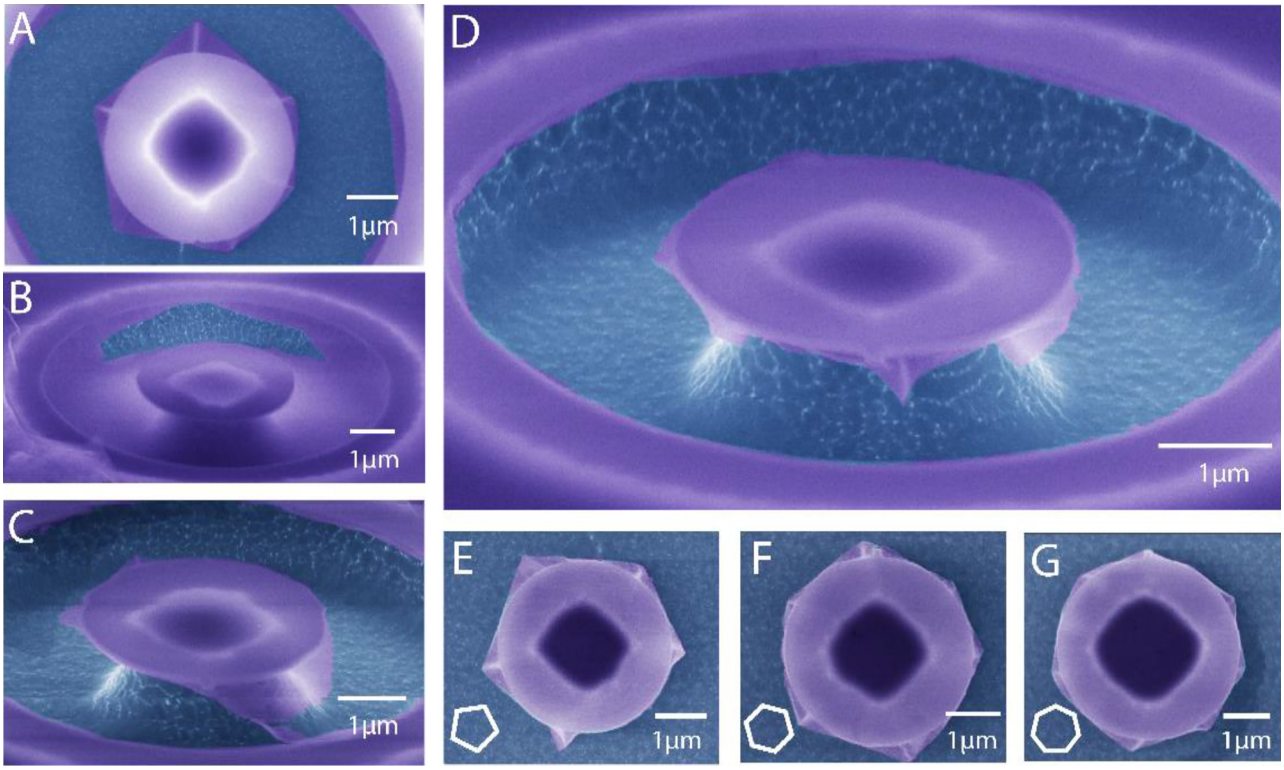


Figure 1: SEM imaging of 20-nm-thick hBN on Si_3N_4 microdisks. (A) 'Tablecloth' configuration with the hBN film falling vertically on the resonator perimeter to make contact with the undercut region. (B) Partially torn hBN film suspended above the undercut. (C) Severely torn, 'tablecloth' configuration. (D) When completely separated from the rest, the hBN film wraps around the microdisk edge. (E-G) Top view of hBN/Si_3N_4 structures similar to that in (D) but with variable film folding geometries displaying 5, 6, and 7 edges respectively. The microdisk diameter is 3.5 µm in (A–F) and 4 µm in (G); all SEM images are false-colored for clarity.

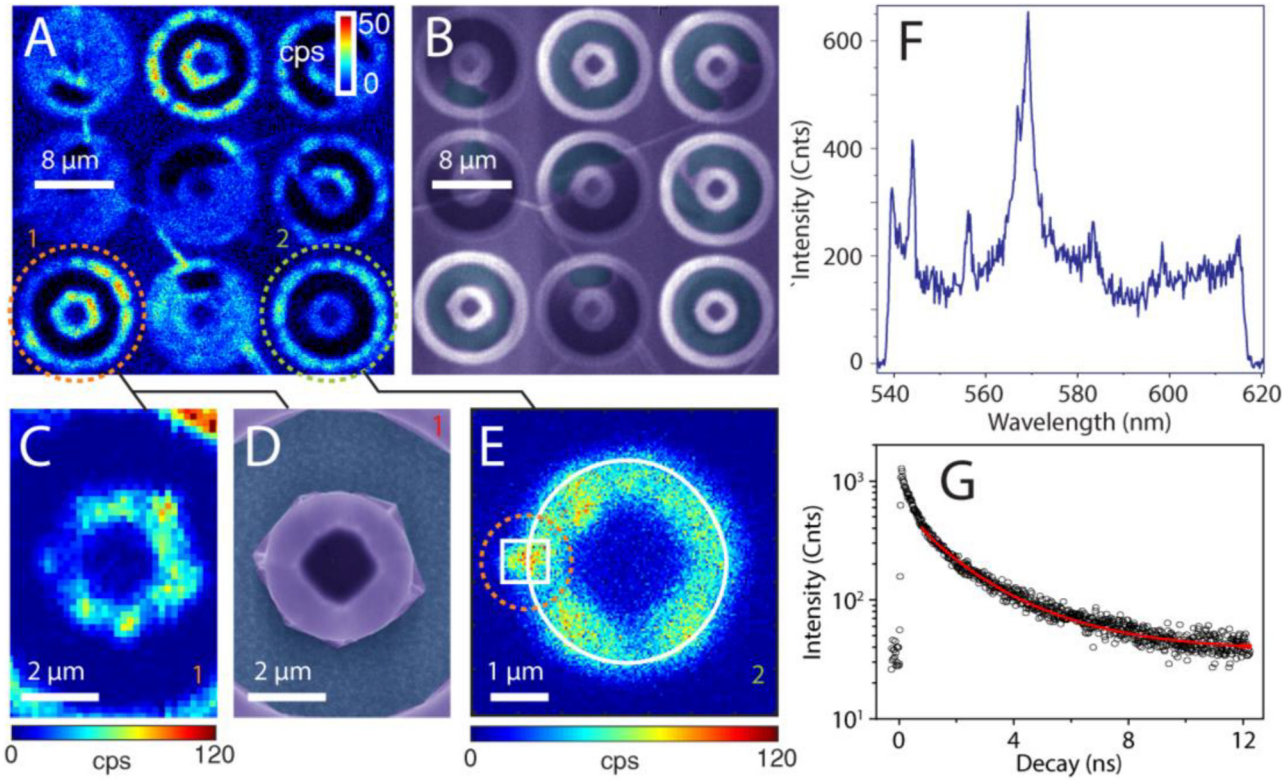


Figure 2: Photoluminescence from strain activated emitters in hBN. (A) Confocal fluorescence image of an array of hBN/Si_3N_4, 3.5-µm-diameter microdisk cavities upon 510 nm laser excitation. At 'wrapped' resonator sites, emission preferentially stems from the microdisk perimeter and the outer contour of the undercut etch. Disks circled as "1" and "2" are surveyed in (C & D) and (E-G), respectively. (B) SEM image of the array shown in (A). (C, D) Zoomed confocal and SEM images of microdisk resonator 1 (lower left corner in (A)). (E) Same as in (C) but for resonator 2 (right lower corner in (A)). Overlaid white circle (square) serves as a guide for the microdisk perimeter (out-coupler location). (F) PL spectra at the out-coupler upon 520 nm, 1 mW laser excitation showing a defect emitter coupled to the WGM resonance. (G) Excited state lifetime measurements of emitters resonant with a cavity mode. The solid red trace is a Gaussian exponential fit (Supplementary Note 3) with a lifetime of 2.28 ± 0.01 ns.

3.2 Interplay between cavity modes and defect state emission

The impact of the WGMs on the emitters' dynamics is not apparent when inspecting the fluorescence brightness, often times uniform along the disk perimeter (Figure 2E). It can be clearly exposed, however, as we compare the spectral properties of light collected from the photon out-coupler at the disk circumference. The spectrum in Figure 2F shows the coupling of emission from a defect emitter to one of the WGMs and hence increase in the emission intensity compared to the other modes. This spectrum is markedly different from the background WGM spectrum observed from the bare Si_3N_4 microdisks shown in Supplementary Figure 1D. Furthermore, the main emission peak observed in Figure 2F is reminiscent of the emission observed previously in strain-activated defects in hBN [28] with the additional spectral narrowing arising from the coupling to the WGMs. We also carried out time resolved PL measurements on similar defects in hBN coupled to WGMs. An example is shown in Figure 2G showing the 'on-resonance' PL transient from photon collection within a small spectral window around 568 nm where we measure a lifetime of 2.28 ± 0.01 ns, comparable to what has been previously observed from such defect emitters [20,28].

Extending the observations above, the experiments in Figure 3 alter our confocal imaging scheme — so far limited to collecting fluorescence from the point of illumination — to one where the excitation and observation loci can be adjusted freely (Figure 3A). This geometry gives us the flexibility to more clearly expose the interplay between the defect emission and the resonator modes. As a first illustration, we set the collection point at the out-

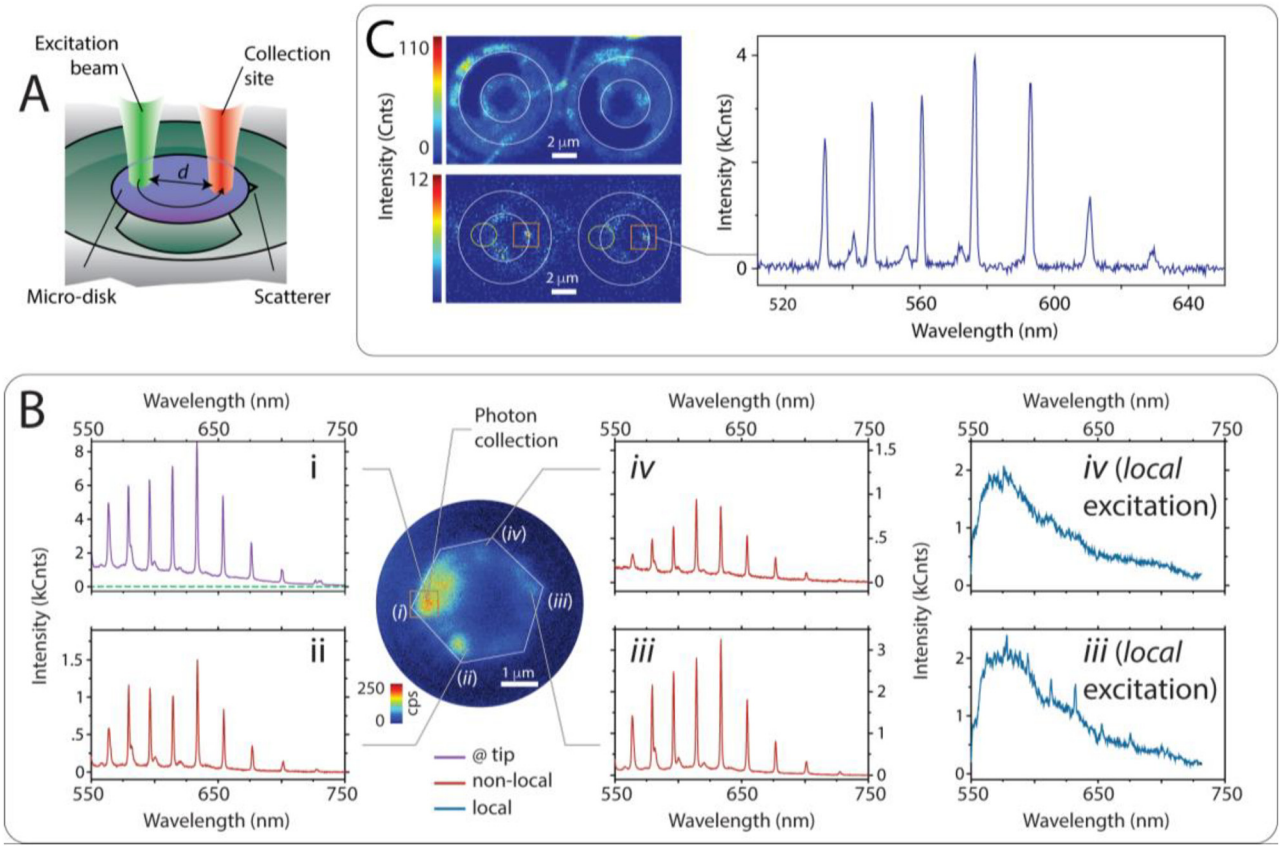


Figure 3: Resonator-mediated photon emission from color centers in hBN. (A) Non-local excitation schematics. (B) (Main) Fluorescence image of an hBN-wrapped micro-disk using the scheme in (A); in this case, photons are collected exclusively at the tip site (orange square, point (i) in the image) while the laser beam scans the rest of the sample. (i) Fluorescence spectrum at site (i), where photon excitation and collection coincide. The green dashed line is the spectrum collected from the bare Si_3N_4 microdisk under similar collection conditions. (ii–iv) Fluorescence spectra upon optical excitation at sites (ii), (iii), and (iv), respectively. Collection of uncoupled emission is considerably suppressed. (Right) Fluorescence spectra at sites (iii) and (iv) obtained via standard confocal microscopy (i. e., co-local excitation and collection). (C) (Top) Standard confocal image of two Si_3N_4 microdisks. (Bottom) Same area as in the top image but for the case where the collection point moves jointly with the excitation point, at a distance *d* nearly matched to the micro-disk diameter. Photons detected at the resonator tip (red square) originate from emitters in the opposite side of the disk (green oval). White traces demark the contours of the resonators and surrounding undercut edges. (Right) Fluorescence spectrum at the out-coupler site featuring near-complete background suppression. The integration time for the spectra above was 30 s.

coupler tip and scan the laser beam across the Si_3N_4/hBN structure hence allowing us to collect the light scattered from the resonator tip as the laser excites the emitters at other points of the microdisk. Figure 3B reproduces the image from a 4-μm-diameter resonator emerging from this non-local excitation scheme: Away from the out-coupler area (orange square), we identify several bright spots across the disk periphery, likely connected to points in the resonator where the hBN film wrinkles or folds, hence allowing the excitation beam to more efficiently couple to the cavity. The corresponding spectra prominently feature the WGM wavelengths with reduced off-resonance contributions (insert Figures (i) through (iv) in 3B). These observations contrast with those obtained at the same sites via standard confocal microscopy (i. e., co-local excitation and collection), characterized by featureless non-resonant photoluminescence stemming from the heterogeneously broadened emitter ensemble [34] (right inserts in Figure 3B). In Figure 3C we use a variant of the above technique where the excitation and collection focal points move jointly, with a fixed separation matched to the disk diameter. Upon properly adapting the scanning trajectory, light collected at the tip exclusively stems from excitation at the opposite side of the disk. The resulting disk-mediated spectrum shows virtually no fluorescence at non-resonant wavelengths.

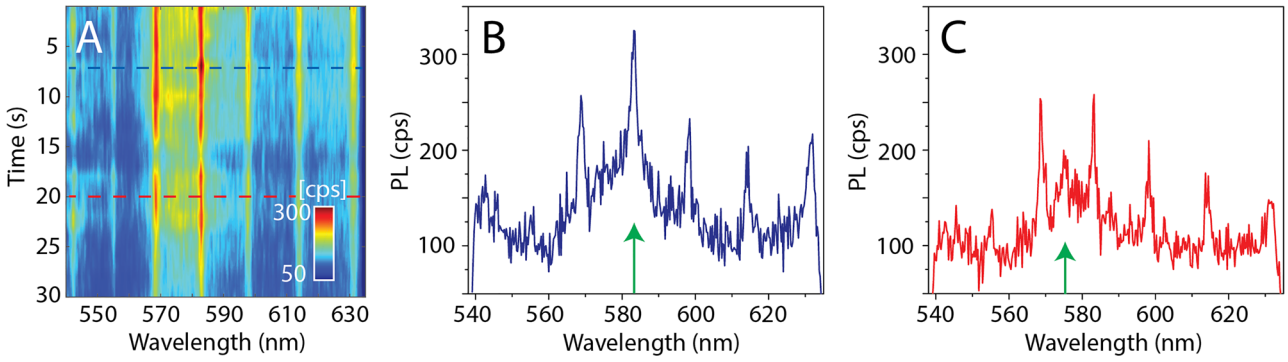


Figure 4: Time trace of hBN emitters coupled to microdisk modes. (A) Fluorescence spectra from a microdisk with an emitter undergoing spectral diffusion and blinking between 564 and 583 nm WGMs; the acquisition time per spectrum is 1 s. (B, C) Line cuts of the time trace in (A) respectively show the case when the emitter is coupled to the 583 nm WGM at 7 s, and when the emission lies between the 564 and 583 nm WGMs at 20 s. The green arrow highlights the emitter's peak position in each case.

These defect emitters are prone to strong spectral diffusion (possibly due to photo-induced charge fluctuations during illumination), which gives us the opportunity to monitor their response as they transiently become resonant with one of the WGMs. One example is shown in Figure 4A, where we display a time series of PL spectra acquired every second during a 30-s-long window. The emitter undergoes fast spectral diffusion and shows blinking as seen in the time traces. Two representative line cuts at 7 and 20 s are shown in Figures 4B and C, respectively. The line cut at 7 s shows the coupling of an emitter to the WGM resonance while at 20 s, the emitter has spectrally drifted from the WGM resonance where the emission is weaker than on resonance. This change could be indicative of resonant enhancement of the defect emission, though additional work will be mandatory to confirm this point. In particular, we note that unlike in prior measurements — where we activated individual color centers via ~75 nm wide pillars [28] — observing photon anti-bunching is difficult in the present configuration due to intermittent spectral overlap with other emitters.

4 Conclusions

In summary, our work introduces a hybrid route to controlling the emission of quantum emitters in micro-resonators 'dressed' by two-dimensional materials. In addition to performing the primary role of enhancing emission through out-coupling via the resonant modes, microdisk resonators also provide the strain needed to activate the defect emitters. These results represent a first step towards developing practical hybrid, chip-scale quantum photonic systems, where the properties of the optically active emitters, their 2D material host, and the supporting, photon-guiding structure can be independently optimized. Indeed, we anticipate several possible extensions, for example, through the use of more compact, smaller-mode-volume beam resonators as a strategy to enhance emitter/cavity coupling, and attain good multiphoton suppression and anti-bunching response. Along the same lines, combining strain-activation and defect engineering (e. g., via focused ion implantation or electron bombardment) may provide a means to generate optically active, spectrally stable emitters at precise locations in otherwise pristine 2D hosts. Finally, extensions to structures comprising tapered fibers or on-chip waveguides evanescently coupled to the resonators should serve as a platform for high-photon extraction and a variety of on-chip cavity quantum electrodynamics experiments.

Acknowledgments: We thank Dr. Daniela Pagliero and Dr. Jacob Henshaw for technical assistance with part of the instrumentation used. N.V.P., G.L.M., and V.M.M. acknowledge support from the NSF ECCS-1906096 and the NSF EFRI 2-DARE program (EFMA -1542863). H.J., G.L.M., and C.A.M acknowledge support from the National Science Foundation through grants NSF-1619896, NSF-1726573, and from Research Corporation for Science Advancement through a FRED Award. All authors acknowledge support from and access to the infrastructure provided by the NSF CREST IDEALS (NSF-1547830) and the CUNY-ASRC Nanofabrication Facility.

References

[1] K. Hennessy, A. Badolato, M. Winger, et al., "Quantum nature of a strongly coupled single quantum dot-cavity system," *Nature*, vol. 445, pp. 896–899, 2007, https://doi.org/10.1038/nature05586.

[2]. R. E. Evans, M. K. Bhaskar, D. D. Sukachev, et al., "Photon-mediated interactions between quantum emitters in a diamond nanocavity," Science, vol. 362, no. 6415, pp. 662–665, 2018, https://doi.org/10.1126/science.aau4691.

[3] S. Sun, H. Kim, Z. Luo, S. Glenn, and E. Waks, "A single-photon switch and transistor enabled by a solid-state quantum memory," *Science*, vol. 361, pp. 57–60, 2018, https://doi.org/10.1126/science.aat3581.

[4] J. L. Zhang, S. Sun, M. J. Burek, et al., "Strongly cavity-enhanced spontaneous emission from silicon-vacancy centers in diamond," *Nano Lett.*, vol. 18, pp. 1360–1365, 2018, https://doi.org/10.1021/acs.nanolett.7b05075.s001.

[5] A. Dousse, J. Suffczyński, A. Beveratos, et al., "Ultrabright source of entangled photon pairs," *Nature*, vol. 466, pp. 217–220, 2010, https://doi.org/10.1038/nature09148.

[6] D. Riedel, I. Söllner, B. J. Shields, et al., "Deterministic enhancement of coherent photon generation from a nitrogen-vacancy center in ultrapure diamond," *Phys. Rev. X*, vol. 7, pp. 1–8, 2017, https://doi.org/10.1103/physrevx.7.031040.

[7] J. L. O'Brien, "Optical quantum computing," *Science*, vol. 318, pp. 1567–1570, 2007, https://doi.org/10.1126/science.1142892.

[8] T. Heindel, C. A. Kessler, M. Rau, et al., "Quantum key distribution using quantum dot single-photon emitting diodes in the red and near infrared spectral range," *New J. Phys.*, vol. 14, 2012, https://doi.org/10.1088/1367-2630/14/8/083001.

[9] P. Michler, A. Kiraz, C. Becher, et al., "A Quantum Dot Single-Photon Turnstile Device," *Science*, vol. 290, 2000, https://doi.org/10.1126/science.290.5500.2282.

[10] B. Lounis and W. E. Moerner, "Single photons on demand from a single molecule at room temperature," *Nature*, vol. 407, pp. 491–493, 2000, https://doi.org/10.1038/35035032.

[11] A. Srivastava, M. Sidler, A. V Allain, D. S. Lembke, A. Kis, and A. Imamo, "Optically active quantum dots in monolayer WSe2," *Nat. Nanotechnol.*, vol. 10, pp. 491–496, 2015, https://doi.org/10.1038/nnano.2015.60.

[12] P. Tonndorf, R. Schmidt, R. Schneider, et al., "Single-photon emission from localized excitons in an atomically thin semiconductor," *Optica*, vol. 2, p. 347, 2015, https://doi.org/10.1364/optica.2.000347.

[13] Y. He, G. Clark, J. R. Schaibley, et al., "Single quantum emitters in monolayer semiconductors," *Nat. Nanotechnol.*, vol. 10, pp. 497–502, 2015, https://doi.org/10.1038/nnano.2015.75.

[14] C. Chakraborty, L. Kinnischtzke, K. M. Goodfellow, R. Beams, and A. N. Vamivakas, "Voltage-controlled quantum light from an atomically thin semiconductor," *Nat. Nanotechnol.*, vol. 10, pp. 507–511, 2015, https://doi.org/10.1038/nnano.2015.79.

[15] M. Koperski, K. Nogajewski, A. Arora, et al., "Single photon emitters in exfoliated WSe2 structures," *Nat. Nanotechnol.*, vol. 10, pp. 503–506, 2015, https://doi.org/10.1038/nnano.2015.67.

[16] A. Faraon, C. Santori, Z. Huang, V. M. Acosta, and R. G. Beausoleil, "Coupling of nitrogen-vacancy centers to photonic crystal cavities in monocrystalline diamond," *Phys. Rev. Lett.*, vol. 109, 2012, https://doi.org/10.1103/physrevlett.109.033604.

[17] B. J. M. Hausmann, B. J. Shields, Q. Quan, et al., "Coupling of NV centers to photonic crystal nanobeams in diamond," *Nano Lett.*, vol. 13, pp. 5791–5796, 2013, https://doi.org/10.1021/nl402174g.

[18] P. E. Barclay, K. M. C. Fu, C. Santori, and R. G. Beausoleil, "Chip-based microcavities coupled to nitrogen-vacancy centers in single crystal diamond," *Appl. Phys. Lett.*, vol. 95, p. 191115, 2009, https://doi.org/10.1063/1.3262948.

[19] D. O. Bracher, X. Zhang, and E. L. Hu, "Selective Purcell enhancement of two closely linked zero-phonon transitions of a silicon carbide color center," *Proc. Natl. Acad. Sci.*, vol. 114, pp. 4060–4065, 2017, https://doi.org/10.1073/pnas.1704219114.

[20] T. T. Tran, K. Bray, M. J. Ford, M. Toth, and I. Aharonovich, "Quantum emission from hexagonal boron nitride monolayers," *Nat. Nanotechnol.*, vol. 11, pp. 37–41, 2016, https://doi.org/10.1038/nnano.2015.242.

[21] Z. Shotan, H. Jayakumar, C. R. Considine, et al., "Photoinduced modification of single-photon emitters in hexagonal boron nitride," *ACS Photonics*, vol. 3, 2016, https://doi.org/10.1021/acsphotonics.6b00736.

[22] T. T. Tran, C. Elbadawi, D. Totonjian, et al., "Robust multicolor single photon emission from point defects in hexagonal boron nitride," *ACS Nano*, vol. 10, pp. 7331–7338, 2016, https://doi.org/10.1021/acsnano.6b03602.

[23] N. R. Jungwirth, B. Calderon, Y. Ji, M. G. Spencer, M. E. Flatt, and G. D. Fuchs, "Temperature dependence of wavelength selectable zero-phonon emission from single defects in hexagonal boron nitride," *Nano Lett.*, vol. 16, pp. 6052–6057, 2016, https://doi.org/10.1021/acs.nanolett.6b01987.

[24] S. A. Tawfik, S. Ali, M. Fronzi, et al., "First-principles investigation of quantum emission from hBN defects," *Nanoscale*, vol. 9, pp. 13575–13582, 2017, https://doi.org/10.1039/c7nr04270a.

[25] G. Grosso, H. Moon, B. Lienhard, et al., "Tunable and high-purity room temperature single-photon emission from atomic defects in hexagonal boron nitride," *Nat. Commun.*, vol. 8, pp. 1–8, 2017, https://doi.org/10.1038/s41467-017-00810-2.

[26] N. Mendelson, M. Doherty, M. Toth, et al., *Strain Engineering of Quantum emitters in Hexagonal Boron Nitride*, arXiv 1911.08072, 2020.

[27] N. Mendelson, Z. Q. Xu, T. T. Tran, et al., "Engineering and tuning of quantum emitters in few-layer hexagonal boron nitride," *ACS Nano*, vol. 13, pp. 3132–3140, 2019, https://doi.org/10.1021/acsnano.8b08511.

[28] N. V Proscia, Z. Shotan, H. Jayakumar, et al., "Near-deterministic activation of room-temperature quantum emitters in hexagonal boron nitride," *Optica*, vol. 5, p. 1128, 2018, https://doi.org/10.1364/optica.5.001128.

[29] T. Vogl, R. Lecamwasam, B. C. Buchler, Y. Lu, and P. K. Lam, "Compact cavity-enhanced single-photon generation with hexagonal boron nitride," *ACS Photonics*, vol. 6, p. 51, 2019, https://doi.org/10.1021/acsphotonics.9b00314.

[30] N. V Proscia, R. J. Collison, C. A. Meriles, and V. M. Menon, "Coupling of deterministically activated quantum emitters in hexagonal boron nitride to plasmonic surface lattice resonances," *Nanophotonics*, vol. 8, 2019, https://doi.org/10.1515/nanoph-2019-0136.
[31] S. Kim, J. E. Fröch, J. Christian, et al., "Photonic crystal cavities from hexagonal boron nitride," *Nat. Commun.*, vol. 9, 2018, https://doi.org/10.1038/s41467-018-05117-4.
[32] M. Nguyen, S. Kim, T. T. Tran, et al., "Nanoassembly of quantum emitters in hexagonal boron nitride and gold nanospheres," *Nanoscale*, vol. 10, pp. 2267–2274, 2018, https://doi.org/10.1039/c7nr08249e.
[33] Y. T. Wang, W. Liu, Z. P. Li, et al., *A Bubble-induced Ultrastable and Robust Single-photon Emitter in Hexagonal Boron Nitride*, arXiv 1906.00493, 2019.
[34] M. Koperski, K. Nogajewski, and M. Potemski, "Single photon emitters in boron nitride: More than a supplementary material," *Opt. Commun.*, vol. 411, pp. 158–165, 2018, https://doi.org/10.1016/j.optcom.2017.10.083.

Supplementary material: Supplementary material to this article can be found online at https://doi.org/10.1515/nanoph-2020-0187.